INSTITUTE OF PHYSICS PUBLISHING and INTERNATIONAL ATOMIC ENERGY AGENCY NUCLEAR FUSION

Nucl. Fusion **46** (2006) 521–531 doi:10.1088/0029-5515/46/5/004

Coupling to the electron Bernstein wave using a phased array of waveguides in MST reversed field pinch

M. Cengher, J.K. Anderson, V. Svidzinski and C.B. Forest

[1] Department of Physics, University of Wisconsin, 1150 University Ave, Madison, WI 53706, USA

E-mail: cbforest@wisc.edu

Received 31 August 2005, accepted for publication 20 February 2006
Published 23 March 2006
Online at stacks.iop.org/NF/46/521

Abstract

Coupling to the electron Bernstein wave (EBW) via a phased array of waveguides is experimentally investigated in the Madison symmetric torus reversed field pinch (RFP). EBWs promise to provide localized heating and current drive in overdense plasmas such as those in the RFP, provided a technique can be developed to efficiently couple power from an externally launched electromagnetic wave to the electrostatic EBW. The choice of antenna structure and launched wave polarization are important factors in coupling waves with frequencies in the electron cyclotron range to EBW, especially on the RFP where the mode conversion to the EBW can take place in the near-field of the antenna. In this paper, a recently developed theory of coupling to EBW from a phased array of waveguides is tested against experiment. The theory predicts that coupling efficiency will vary with launch angle and that coupling depends sensitively upon the edge density profile. Amplitudes and phases of reflected power in each of the waveguides are measured experimentally and compared with predictions based upon density profiles measured by a Langmuir probe in the edge of the plasma. The parametric dependence of reflection has been studied for different polarizations, different launch angles, time varying density profiles and several frequencies of the launched wave. An asymmetry in reflection versus the launch angle predicted by theory was found experimentally for the X-mode, while the O-mode was symmetric. The dependence on density scale length predicted by theory was confirmed in the experiment. The phase of the reflected signal is shown to contain reflectometry-based information about the edge density profile. For appropriate phasing, measurements show that the total power reflection coefficient can be lower than 15%.

PACS numbers: 52.35.Hr, 52.35.Mw, 52.40.Fd, 52.50.Sw, 52.70.Gw

(Some figures in this article are in colour only in the electronic version)

1. Introduction

Radiofrequency waves in the electron cyclotron range of frequencies (ECRFs) are well suited to heating and driving current in fusion plasmas. When the plasma is underdense ($\omega_{pe} < \omega_{ce}$), an extraordinary (X) mode or ordinary (O) mode launched from the edge of the plasma (at frequencies above cutoff) can propagate inside the plasma and transfer the wave energy to electrons.

For overdense plasmas ($\omega_{pe} > \omega_{ce}$ for most of the plasma section, except for a small region at the edge), waves in the ECRF are cutoff in the low-density outboard edge region of the plasma and do not penetrate into the plasma core. The O-mode cutoff occurs at the electron plasma frequency ($\omega = \omega_{pe}$) and the X-mode features the right and left cutoffs ($\omega_{R,L} = (1/2)[\sqrt{\omega_{pe}^2 + 4\omega_{ce}^2} \pm |\omega_{ce}|]$). Theoretical studies have shown that waves in the ECRF can propagate beyond the edge by mode conversion to the electrostatic electron Bernstein wave (EBW) [1] which propagates only in overdense plasmas. Scenarios for coupling from electromagnetic waves to the EBW in overdense fusion plasmas were proposed in [2–5]. Early experiments in small laboratory plasmas have confirmed the generation and propagation of the EBW [6–8] and verified the basic mode conversion process. Recent experiments in a linear plasma system [9] show an appreciable power mode conversion efficiency of 85% from ECRF to EBW.

Early theoretical studies [10–12] and experimental studies [13, 14] of EBW propagation in plasma slabs have both shown that EBWs are sustained by electron cyclotron motion, do not have any density cutoffs inside the plasma and can

propagate without an upper density limit. Moreover, the EBW experiences very localized damping on electrons near the electron cyclotron resonance or its harmonics. Numerical modelling has shown that localized current drive and heating is possible in plasmas such as the reversed field pinch (RFP) and spherical tokamak (ST), with the direction of the EBW-driven current being controlled by the angle of launching in the poloidal plane [15, 16].

Several scenarios are generally considered for coupling to EBW. The first scenario is high field side XB: the slow X-mode launched from the high field side converts to EBW at the upper hybrid resonance ($\omega_{\mathrm{UH}} = \sqrt{\omega_{\mathrm{pe}}^2 + \omega_{\mathrm{ce}}^2}$). It is the most straightforward, and is often an implicit part of conventional ECRF heating [15, 17, 18]. EBW current drive was measured for the X-mode launched from the high field side in the COMPASS-D tokamak [17].

The second is known by the acronym OXB, a double mode conversion scenario where an obliquely launched O-mode tunnels to the slow branch of the X-mode which in turn converts to the EBW. Using this scenario, emission, heating and current drive were observed in overdense stellarator plasmas [19, 20]. The third is low field side XB, where the fast X-mode is launched at the plasma boundary at a finite angle and tunnels through the evanescent layer between right cutoff and upper hybrid resonance to couple to the EBW. It must be noted that for oblique launch the waves with initial X and O polarizations at the antenna opening (rf wave electric field perpendicular, respectively, parallel to the plasma edge magnetic field) become a mixed X/O mode as the wave propagates into the plasma.

The emphasis of this paper is on coupling to the EBW in the demanding environment of the RFP. The theoretical prediction that plane wave coupling to EBW is increased in the XB mode for oblique launch [21, 22] motivated a study of the possibility of using a phased array antenna on the RFP [5]. Previous experiments have measured ECRF emission of the X- and the O-mode from MST plasmas, coming from mode-converted EBWs [23], and has shown by reciprocity the possibility of heating the plasma. Here, coupling to the EBW is studied with a focus on finding a suitable launch geometry and RFP plasma conditions for optimized coupling of the applied power to the EBW using a phased array of waveguides. This approach has strong similarities to the technique used for coupling to the lower hybrid waves in tokamaks [24]. In this paper we give an overview of the RFP geometry, edge conditions, etc, which motivate the present experiments. We then review the plane wave theory of coupling ECRF waves to EBW in overdense plasmas in section 2 with emphasis on the particular MST parameters. Coupling depends on a large set of plasma and wave parameters, such as edge density profile characteristics, magnetic field strength, applied frequency, the launched mode (X and O), perpendicular wave number and antenna geometry. In section 3 the theoretical approach used for predicting the power reflection coefficient and phase for different launching configurations and plasma conditions is presented. Optimum coupling conditions were found from these simulations. Experimental measurements of power reflection are then discussed in section 4 and compared with theory.

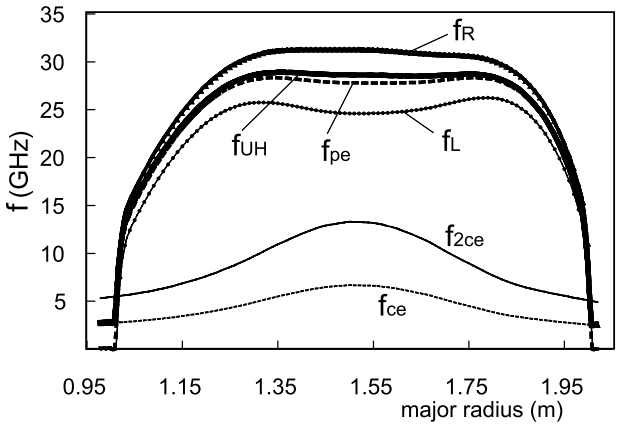

Figure 1. The characteristic cold plasma frequencies in the ECRF plotted versus major radius in the MST RFP ($I_{\mathrm{p}} \sim 200$ kA): f_{pe} (- - - -), f_{ce} (- - - -), $f_{2\mathrm{ce}}$ (——), f_{uh} (——), f_R (—▲—) and f_L (●).

Both theory and experiment converge in showing the optimum conditions in which RFP plasmas can be heated by the EBW. The outboard launch of the X-mode with a dielectric-covered phased array antenna leads to coupling sufficient for a heating experiment: optimum coupling is found in quiescent plasmas [25] with the reflected fraction routinely less than 20% for a particular inter-guide phase to set the ideal launch angle.

2. Background: EBWs in the RFP

The RFP has a unique magnetic geometry which impacts rf heating and current drive. The magnetic field at the edge is almost entirely poloidal, generated by plasma current, and varies weakly with minor radius, and the surfaces of constant $|B|$ are nearly aligned with the magnetic flux surfaces. Electromagnetic waves in the ECRF can propagate only in the edge of these plasmas, since the ratio of the electron plasma frequency f_{pe} to the electron cyclotron frequency f_{ce} is well above unity over most of the plasma cross section (figure 1). The left and right cutoffs, upper hybrid resonance and O-mode cutoff in the MST poloidal section are shaped like concentric circles. The Madison symmetric torus (MST) RFP has a major radius $R = 1.5$ m and a minor radius of 0.52 m [26] and $f_{\mathrm{pe}}/f_{\mathrm{ce}} > 5$ in the core of the plasma as shown in figure 1 where the frequencies in the poloidal cross section are plotted versus the machine radius for a 210 kA plasma. Typical parameters for low plasma current MST discharges (also used in the computational work) were $I_{\mathrm{p}} = 180$–260 kA, $n_{\mathrm{e}} = 0.4 \times 10^{13}$–$1.2 \times 10^{13}$ cm^{-3}, $|B|(a) = 0.07$–0.1 T and very specific edge parameters discussed below. This work is focused on low current discharges (lower Ohmic heating power $P_\Omega \sim 2$ MW and electron temperature $T_{\mathrm{e}} \sim 200$ eV) because the corresponding electron cyclotron resonance is conveniently placed in the S-band where high power sources are available. The levels of ECRF power launched were well below the ohmic power, so no heating or current drive effects are expected to be measured in these coupling experiments. The experiments have focused on a frequency of 3.6 GHz which places the resonance near the centre of the plasma for $I_{\mathrm{p}} = 180$ kA and near the edge for $I_{\mathrm{p}} = 300$ kA. In addition to the available heating power, the S-band waveguide antenna fits through existing circular ports on MST.

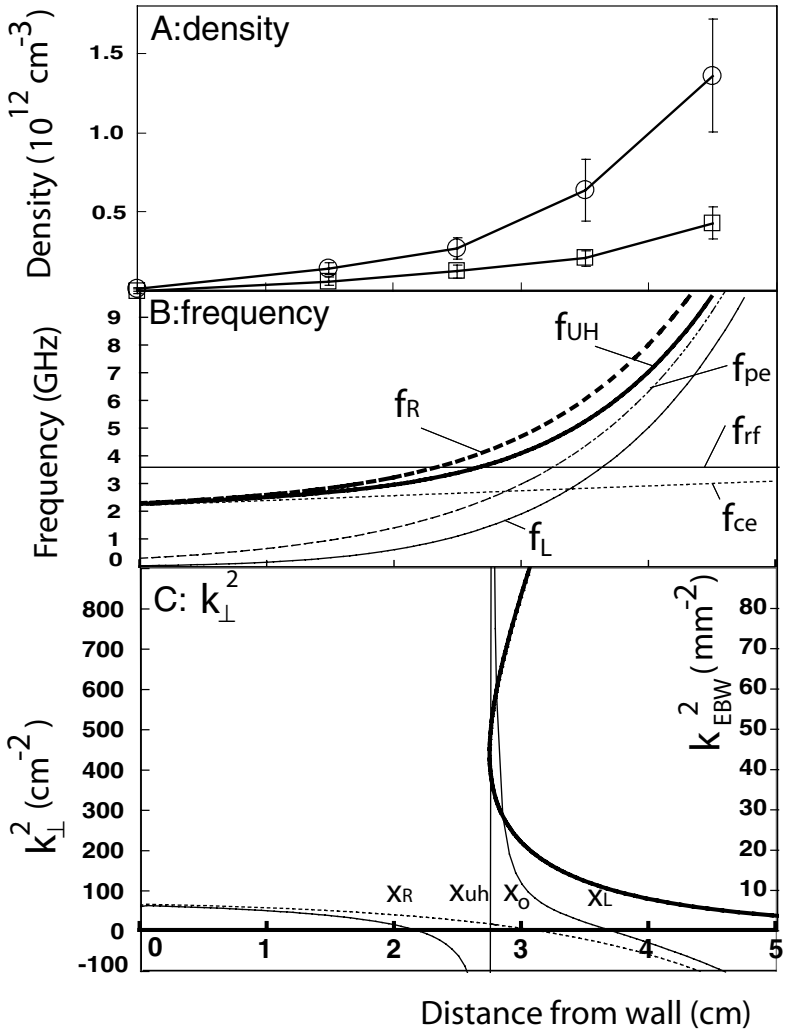

Figure 2. (*a*) Measured density profiles for standard plasma in MST (○) and PPCD (□) for the first 5 cm from MST wall, averaged over 0.25 ms. (*b*) frequencies in the extreme edge region corresponding to the PPCD profile in (*a*): f_{pe} (— · —), f_{ce} (- - - -), f_{uh} (——), f_R (**- - - -**) and f_L (——) versus the distance from the MST wall. (*c*) Plot of the roots of the dispersion relation at $f = 3.6$ GHz for the RFP plasma. Cold plasma dispersion roots for O-mode are plotted with the dashed line, for the X-mode with a thin continuous line and hot plasma EBW dispersion first harmonics roots with a thick continuous line.

Coupling to the EBW takes place in the near-field of the antenna as illustrated in figure 2. Two typical measured edge density profiles corresponding to different edge conditions are plotted in figure 2(*a*). Pulsed poloidal current drive (PPCD), characterized by low fluctuations [27], is a regime of special interest for coupling EBW due to the lower edge density [25] and offers an alternative to standard plasma density profiles. In standard plasmas (and to a lesser degree in PPCD) the density profile in the vicinity of the close fitting conducting wall changes continuously during a discharge, with large fluctuations in MST. This potentially leads to changes in the power reflection as the position of the upper hybrid layer (UHL) and density scale length $L_n = [n_e/(\partial n_e/\partial x)]_{UHL}$ change during the discharge. The intersection of the f_{uh} curve with the wave frequency (3.6 GHz) determines the position of the UHL where mode conversion occurs. Note that the x-axis (radially in from the antenna in the poloidal section) scale is 5 cm in these graphs, which corresponds to $r/a > 0.9$, and is within one vacuum wavelength (8.3 cm for the 3.6 GHz launched wave) of the antenna. Figure 2(*c*) is a plot of the roots of the cold plasma dispersion relation for the same conditions together with the hot plasma EBW first harmonic solution.

The XB scenario starts with the launching of the X-mode at the plasma edge ($x = 0$). The fast X-mode propagates from the plasma edge to the right-hand cutoff. Transmission through the evanescent layer ($x_R < x < x_{uh}$) is strongly related to the density gradient L_n in this region. If this layer is narrow the transmission is high and there is substantial tunnelling of the fast X-mode to the slow X-mode and EBW. The wave propagates to the left-hand cutoff at x_L, where it is reflected back toward the UHL where mode conversion to EBW occurs. This triplet of cutoff–resonance–cutoff forms a mode conversion resonator that leads to efficient coupling to the EBW.

The OXB mode conversion scenario starts with an O-mode propagating from the plasma boundary which couples to the slow branch of the X-mode (plotted in figure 2(*c*)). The cutoff for the O-mode is at x_O, and when this is close to the slow mode cutoff at x_L the coupling can be high since the evanescent layer is small. After energy is transferred to the slow rbanch of the X-mode, the wave travels towards x_{uh} and mode converts to

EBW at the UHL (position of UHL plotted in figure 2(*c*)). Both coupling schemes work in MST-like conditions.

One can compute the mode conversion efficiency for a plane wave propagating in a plasma slab. Assuming a normally incident plane wave, Ram *et al* [28] calculated the maximum conversion efficiency for the XB scenario to be

$$C_{\max} = 4\mathrm{e}^{-\pi\eta}(1 - \mathrm{e}^{-\pi\eta}), \tag{1}$$

where

$$\eta = \frac{\omega_{\mathrm{pe}} L_n}{c} \frac{\alpha}{\sqrt{\alpha^2 + 2(L_n/L_B)}} \left[\frac{\sqrt{1+\alpha^2} - 1}{\alpha^2 + (L_n/L_B)\sqrt{1+\alpha^2}} \right]^{1/2}, \tag{2}$$

$$\alpha = \left[\frac{\omega_{\mathrm{pe}}}{\omega_{\mathrm{ce}}} \right]_{\mathrm{UHR}} \tag{3}$$

and the magnetic field gradient scale length is $L_B = [B/(\partial B/\partial x)]_{\mathrm{UHL}}$.

For magnetic field and density measurements on MST this model predicts that the maximum coupling can reach 100% for $L_n \sim 1$ cm (at $B = 0.07$ T) and that coupling varies sensitively with edge density characteristics.

The theory shows that coupling efficiency is very sensitive to the electron density profile in the near field of the antenna. In general, a steeper gradient places the resonance and cutoff layers close together to allow a higher fraction of the incident energy to tunnel to EBW. Typical MST discharges studied in this work have edge density profiles that vary in time, and often there are several-millisecond periods of dramatically changed edge dynamics (the PPCD experiment [25]). A sample discharge is shown in figure 3: the plasma current (figure 3(*a*)) has a maximum of 200 kA and the line averaged density (figure 3(*b*)) ranges from (0.5–1.2) $\times 10^{13}$ cm^{-3}. The position of the UHL (figure 3(*d*)) and the density scale length at the UHL (figure 3(*e*)) are shown versus time along with a measured edge density (at $x = 2.5$ cm, figure 3(*c*)). The period from 10 to 20 ms is a low fluctuation period (observed in figure 3(*c*)), and during this time L_n is relatively constant around 1.3 cm. The position of the UHL slowly shifts outwards or inwards, and as shown in section 4 this period typically leads to good coupling to EBW. In a standard RFP plasma ($t < 10$ ms or $t > 20$ ms), the density scale length varies rapidly with time and can have significantly higher values (corresponding to a flatter edge density profile) expected to result in less effective coupling. Also, the edge density during the standard phase can be considerably higher, bringing the upper hybrid resonance very close to the plasma boundary (as seen during the period from 25 to 35 ms in figure 3(*e*)), and hence very near the antenna opening.

The plane wave approach, while useful, is not adequate for computing the coupling efficiency in the experiment. Any real antenna has a finite (k_y,k_z) spectrum and a near field that must be considered in the theoretical modelling. Also, the WKB approximation used to describe the wave fields outside the mode conversion region in the above results seem to be invalid in the relatively small plasma edge region where the coupling occurs in the experiment. This work considers in detail a simple waveguide grill: a pair of adjacent waveguides with electronic control of the phase between waves in each arm. The inter-guide phasing is used to tune the launch angle and thus

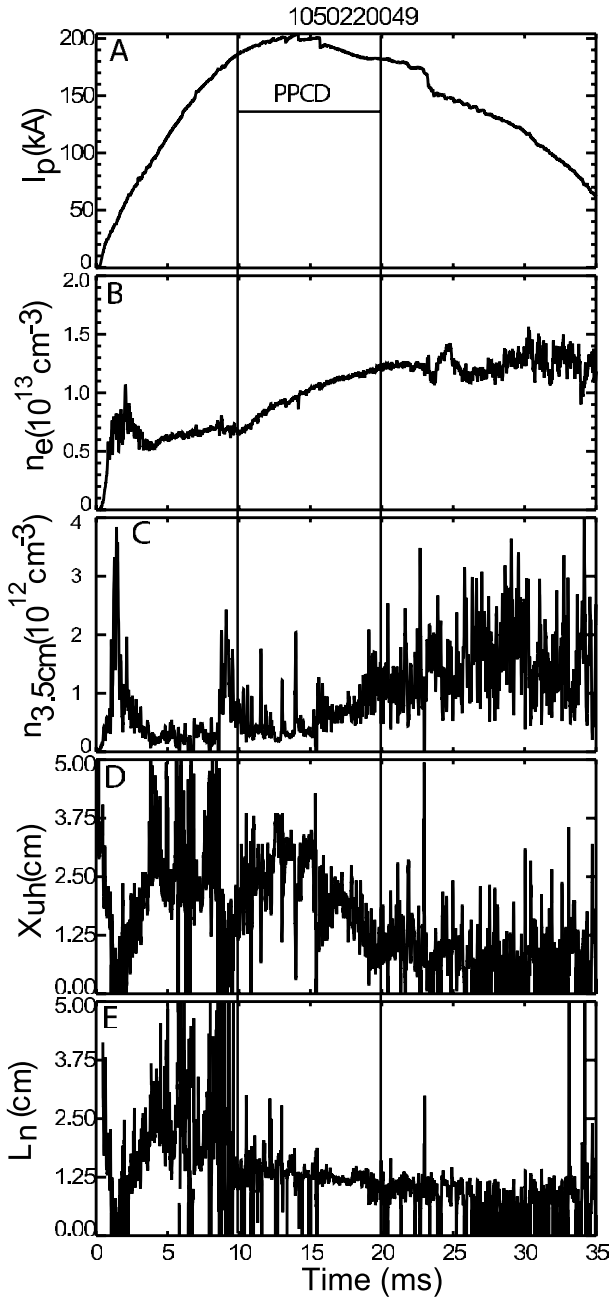

Figure 3. Typical time evolution of current, line average density, edge electron density at 3.5 cm, position of the UHL and L_n during a typical RFP discharge studied in this work.

allows a great flexibility and the possibility of a continuous scan during a discharge. The wave launch angle is a major means to optimize coupling (in addition to the plasma edge density) for either X- or O-mode launch. The rigorous computation treatment of this antenna is discussed in the next section.

3. Theory

A detailed numerical model is required to accurately predict the coupling to the EBW. To carry out this computation, an approach similar to that used successfully for modelling coupling from grill antennas to the lower hybrid wave is used [24]. The geometry used here to model the plasma is

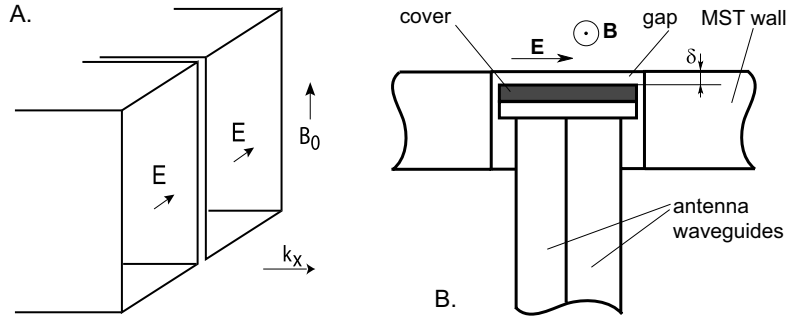

Figure 4. (*a*) Drawing of the twin waveguide antenna. (*b*) Schematic drawing of retractable waveguide array antenna mounted on MST chamber with BN cover and position with respect to MST wall δ.

a one-dimensional slab in which plasma occupies the region $x > 0$. The plasma density and the magnitude and direction of magnetic field are arbitrary functions of the x coordinate while the plasma is uniform in the y and z directions. Identical, rectangular waveguides are taken to form apertures in an infinite, perfectly conducting ground plane located at $x = 0$. The wave propagation in the plasma region is found by solving the Maxwell equations numerically assuming time dependence $\propto \exp(-\mathrm{i}\omega t)$ and using the cold plasma dielectric tensor (which depends on x).

The upper hybrid resonance is resolved by electron collisions. In the limit of small collisionality the total wave absorption at the resonance is independent of collision frequency and the absorbed power is interpreted as the wave power converted to EBW (which happens in the hot plasma model). The justification of such interpretation is provided in [5] where the direct quantitative comparison of cold and hot plasma models is made.

The plasma physics of the problem is entirely described by the 2×2 spectral surface admittance matrix $Y_{ij}(k_y, k_z)$, $i, j = 1, 2$ which relates the tangential electric and magnetic field components at the plasma surface:

$$\begin{pmatrix} B_y \\ B_z \end{pmatrix}_{x=0+} = \begin{pmatrix} Y_{11} & Y_{12} \\ Y_{21} & Y_{22} \end{pmatrix} \begin{pmatrix} E_y \\ E_z \end{pmatrix}_{x=0+}. \qquad (4)$$

To find the admittance matrix we find the magnetic field components at $x = 0$ from the solution of wave equations (using a cold plasma dielectric tensor) in the region $0 < x < x_{\mathrm{end}}$ subject to boundary conditions on electric field amplitudes at $x = 0$ and $x = x_{\mathrm{end}}$. At $x = 0$ we impose two independent boundary conditions (relating to different columns in Y) $E_y = 1$, $E_z = 0$ and $E_y = 0$, $E_z = 1$ and we assume that at $x = x_{\mathrm{end}}$ there is only a wave which either propagates or decays in positive x direction (radiation condition). Point $x = x_{\mathrm{end}}$ is chosen far enough such that the result does not change if one moves it further (this condition is easily satisfied in our case because waves are decaying for large enough x).

The admittance matrix calculated for a spectrum of k_y, k_z values on the plasma side is used to match the plasma to the waveguide array. Note that the waveguide supports the propagation of only a single mode, all higher order modes are evanescent. In the experiment the launcher consists of either a single or a pair of modified S-band waveguides, the dimensions of each guide being 7.21 cm $\times$ 3.454 cm. In the case of a pair, two guides are stacked along the longer dimension of the guide, with a septum of width 0.406 cm between the openings, as in figure 4(*a*). The result of the calculation is the predicted reflection coefficient and phase difference between forward and reflected waves in each waveguide. These parameters are measured in the experiment.

X-mode, O-mode and intermediate angle launch were made possible with antenna rotation around an axis parallel to the propagation direction, so the antenna electric field can be perpendicular to the edge poloidal magnetic field in X-mode as in figure 4(*a*) or parallel to the magnetic field for O-mode. The model is only an approximation to the real launching geometry. The experimental configuration is a 3D toroidal aluminium wall, with the circular port opening, different from the infinite perfectly conducting 2D metallic sheet with rectangular openings assumption. A boron nitride antenna cover, used in several experiments to prevent plasma from entering the antenna, is not included in the model. The edge density used as input in the simulation is measured some distance away and not exactly in front of the antenna. The changes in the MST edge magnetic field configuration due to the presence of the antenna and the MST circular port were only partially included.

For parametric studies of the theoretically predicted coupling for a variety of density profiles, an exponential density profile of the form:

$$n = n_0 \exp[(x - x_0)/L_0], \qquad (5)$$

was used, where L_0 is a parameter used to characterize the density scale length of the profile and x_0 is used to adjust the position of the upper hybrid resonance. We furthermore assumed that the magnetic field which was mainly poloidal in the edge region was of the form $B = (\mu_0 I/2\pi(a-x))$, the fall-off being characteristic of the magnetic field strength fall-off in the MST shell. Here, I = plasma current, a = minor radius and x = distance from plasma edge. Simulations were used to predict the power reflection coefficient, the reflection in each arm R_i/F_i (where F_i is the forward power, R_i is the reflected power and $i = 1, 2$ for the left and the right arm, respectively, of the antenna) and the phases of the reflected waves $\Phi_{F_i R_i} = \Phi_{R_i} - \Phi_{F_i}$. Different conditions were investigated: different frequencies of the propagating wave, single or twin waveguide, ordinary and extraordinary mode, different ratio of the powers for twin waveguide, different positions of the UHL, different density scale lengths at the UHL and the use of phasing

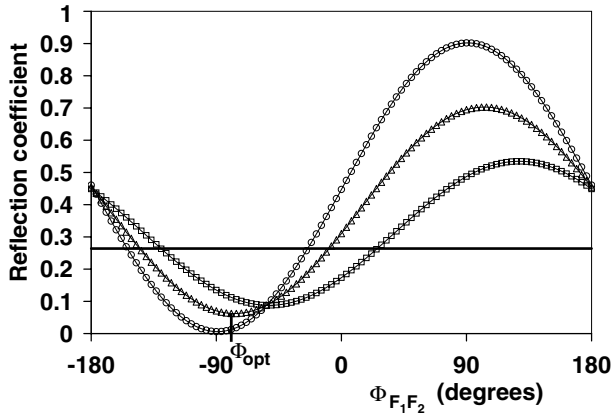

Figure 5. Vacuum calibration tests: (*a*) Measured power reflection coefficient versus phase between waveguides for waves launched in vacuum without cover (○), with smooth boron nitride cover (□), with grooved boron nitride cover (◇), and predicted from simulation (——) (*b*) Reflection coefficient versus inter-guide phase for antenna with no cover at the MST wall (○), antenna retracted 1 cm behind MST wall (△), antenna 1 cm in the MST chamber (×) and predicted from simulation (——).

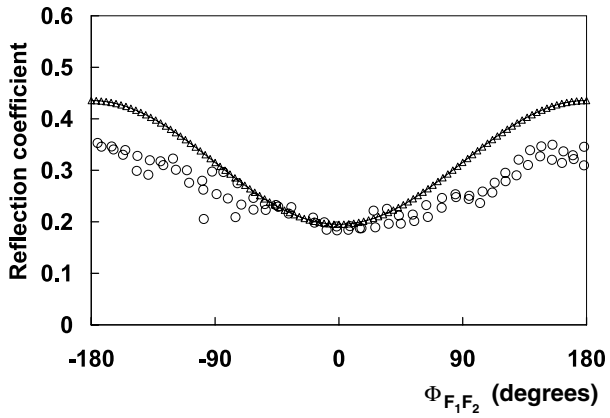

Figure 7. Theoretical X-mode reflection coefficients in plasma versus the phase between the waveguides for a density profile equation (5) with $n_0 = 1 \times 10^{11}$ cm^{-3}, $L_0 = 1.45$ cm, $x_0 = 3.5$ cm and current $I = 190$ kA. Single waveguide (——), twin waveguide (△) and reflection in each arm for the twin waveguide (squares for arm 1, circles for arm 2).

between twin waveguides $\Phi_{F_1F_2} = \Phi_{F_1} - \Phi_{F_2}$. For the single waveguide launch case, the geometry considered was the one used in experiment: one of the twin waveguide antenna arms passive and power being launched through the other arm. The experimentally measured MST parameters of density and magnetic field profiles can also be used as input to the code for comparison between theory and experiment. The edge density profile changes during the time evolution of a typical RFP discharge. At each moment a (L_n, $x_{\rm UH}$) pair can be used to characterize the density profile. Other plasma parameters (plasma current, edge magnetic field, magnetic field pitch angle) are also measured and used as input in the model.

An important prediction of the simulation is that lower reflection can be attained launching X-mode waves through a twin waveguide antenna compared with a single waveguide. A typical dependence of the X-mode total power reflection coefficient on the phasing between the two waveguides can be observed in figure 5. The curve is asymmetric with respect to zero phasing, due to an up–down asymmetry in the Y matrix with respect to the direction mutually perpendicular to the magnetic field and x direction, which is due to the off-diagonal components in the dielectric tensor of a magnetized plasma. This means that a low reflection can be achieved with a proper phasing between the two waveguides (oblique launching angle). The power reflection coefficients for each arm are also presented in figure 5. For the X-mode the use of a single waveguide leads to a higher reflection coefficient than the minimum reflection for the twin waveguide. The asymmetric behaviour of X-mode launch was also predicted for ion Bernstein waves [29]. The theoretical vacuum reflection plotted in figures 6(*a*) and (*b*) is symmetric with respect to zero degrees. The predicted O-mode reflection (figure 7) has also a symmetrical dependence on the interwaveguide phase. Since for RFP the left cutoff and the O-mode cutoff are almost concentric circles in the poloidal plane, an O-mode wave launched perpendicular in the poloidal section encounters the smallest distance between the O-mode cutoff and the left cutoff; so it satisfies the condition for optimum conversion from the O-mode to the slow X-mode in plasma. The minimum possible reflection for the given plasma density and magnetic field profiles in the O-mode using twin waveguide is predicted to be close to the O-mode single waveguide reflection. Comparison of the minimum reflection attainable in each configuration (X-mode in figure 5 and O-mode in figure 7) shows that XB scenario using phased waveguide array can lead to the highest coupling for MST.

The numerical model was used to predict the dependence of the power reflection coefficient on the density scale length at the UHL and wave frequency. The twin waveguide minimum power reflection coefficient is plotted in figure 8 versus the density scale length and wave frequency. The reflection is minimized for density scale length between 0.8 and 1.5 cm in the 3.3–3.9 GHz range of frequencies. Reflection increases strongly as L_n decreases for $L_n < 0.7$ cm, while the increase in reflection with L_n is slower for $L_n > 1.5$ cm. These data verify the optimization predicted in equation (1) (with $\eta \propto L_n$) where the coupling goes to zero in the limit of both long and short density scalelengths. In order to maximize the coupling to the plasma, the phase that gives a minimum total reflection must be selected and will be referred to as optimum phase ($\phi_{\rm opt}$). This information can be used in experiments to adjust the phases in the rf circuit so an optimum coupling can be attained. The dependence of $\phi_{\rm opt}$ on wave frequency and density scale length at the UHL is also plotted in figure 8. A low minimum reflection (below 10%) is predicted for a rather broad range of L_n (0.8–1.5 cm) and frequencies (3.2–3.9 GHz) if the inter-guide phase is set at the optimum value ($\phi_{\rm opt} \sim 0$ to -80) for the particular frequency and L_n. The lowest theoretical reflection coefficient of 0.05 is attained at 3.75 GHz and corresponds to a $\phi_{\rm opt}$ of -85°.

The value of the optimum phase $\phi_{\rm opt}$ also depends on the position of the UHL. For frequencies between 3.0 and 3.9 GHz $\phi_{\rm opt}$ decreases about 20° for $x_{\rm UH}$ from the edge to 3.5 cm, then increases 60–80° (depending on the wave frequency) for $x_{\rm UH}$ from 3.5 to 5.5 cm. Optimum phase dependence with $x_{\rm UH}$ in the O-mode is similar to the X-mode, showing a variation of about 50° cm^{-1} slope.

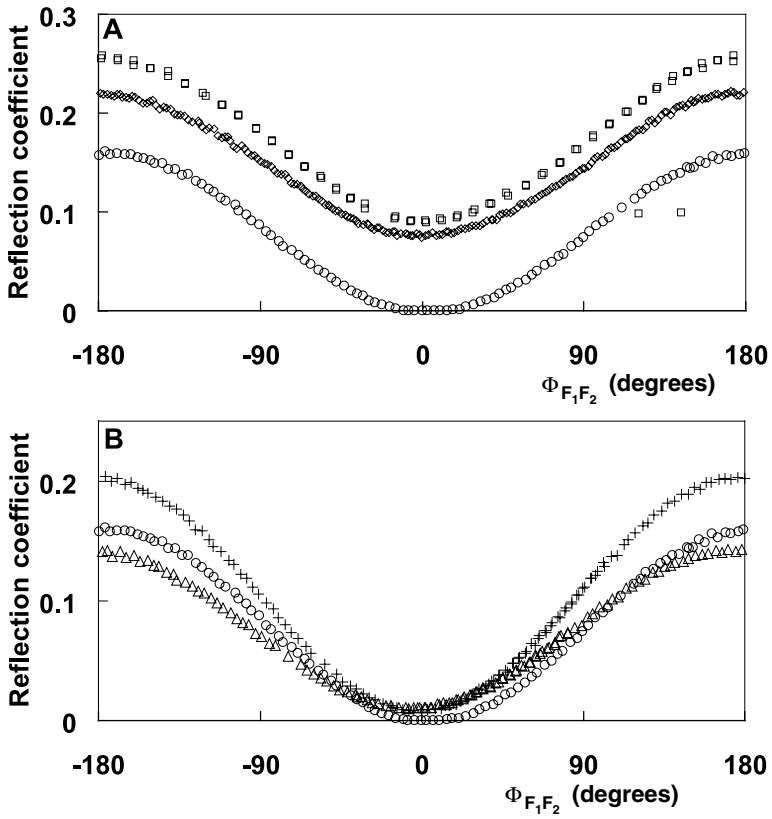

Figure 6. Measured power reflection coefficient versus phase between waveguides for an O-mode wave launched in a 190 kA plasma with boron nitride cover (○) $f = 3.6$ GHz and computation (△) for a density profile equation (5) with $n_0 = 1 \times 10^{11}$ cm^{-3}, $L_0 = 1.45$ cm, $x_0 = 3.5$ cm and current $I = 190$ kA.

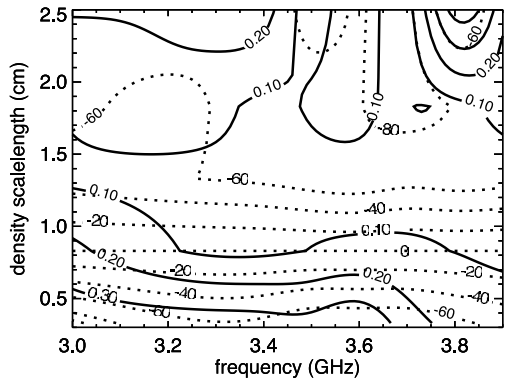

Figure 8. Simulation of X-mode launched with twin waveguide: dependence of the minimum value of the power reflection coefficient (——) and the optimum phasing between the waveguides (- - - -) on the wave frequency and density scalelength. Thick contour shows the lowest value (0.05) of the power reflection coefficient.

In the O-mode launch the electric field is parallel with the magnetic field and this eliminates the up–down asymmetry observed for the X-mode; so the power reflection coefficient is symmetric with respect to zero phasing. Simulation predicts that the use of twin waveguide for the O-mode improves reflection only 5% compared with the single waveguide case, except for very low density scale lengths (below 0.5 cm for 3.6 GHz and position of UHL at 1.5 cm).

A larger array of profiles was investigated in theory, beyond those corresponding to optimal MST parameters. It must be stressed that the above considerations apply to the typical MST profiles with emphasis on the PPCD regime. For these conditions, X-mode launch using a phased array of waveguides is shown to lead to minimum reflection. It was found that in theory the single waveguide had consistently lower or equal coupling compared with the optimum for phased array in X-mode. Theory also shows that the phased array is slightly better than a single waveguide for O-mode launch in a PPCD-like regime, but is not necessarily a better choice for other L_n and x_{UH} ranges.

4. Experimental measurement of coupling

Experimental tests of the waveguide coupling scheme were performed using the two-waveguide grill antenna shown in figure 4(*b*) positioned near the inner surface of the MST vacuum vessel. The relative position of the antenna opening with respect to the MST wall is adjustable and different BN windows (needed to prevent the plasma from entering the waveguides) have been tested. A microwave circuit (figure 9) is used to deliver from around 1 W up to 50 kW of 3.6 GHz rf power to the arms: the output of synthesized function generator is amplified by a travelling wave tube. An isolator prevents reflected power from reaching the tube, and a bidirectional coupler samples forwardand reflected power in each arm. A heterodyne phase detection scheme (455 kHz IF) is used to measure phase differences between waves using digital complex demodulation [30]. The inter-guide phasing is a key

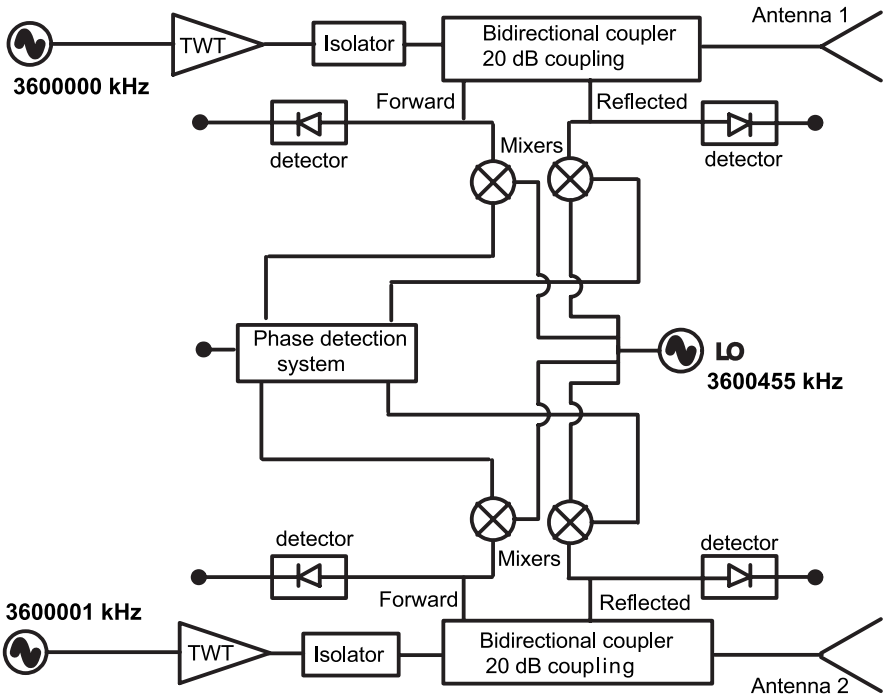

Figure 9. Microwave circuit for reflection and phase measurements for 1–10 W power launched from the two-waveguide antenna. For higher power experiments a second TWT amplifier is used in each arm with 50 dB coupling for power samples.

parameter in determining the spectrum of the launched wave. This is controlled by either introducing a mechanical shift in one arm of the antenna or (as in most of the experiments) by applying slightly different frequency (e.g. $\Delta f = 1$–10 kHz) wave in each waveguide, giving a continuous phase scan. A rotational mounting system allows launch with the O-mode, the X-mode and intermediate polarizations.

A radial array of five Langmuir probes drawing ion saturation current is used to measure the density scale length. The edge density profile is measured with 1 cm resolution and together with the measured plasma current is used to compute the position of the UHL and the density gradient scale length (L_n) at the UHL.

The primary rf signals for the experiments are shown versus time for a typical discharge in figure 10. The forward and reflected power in each arm and the phase between launched and received wave (figure 10(*a*)–(*c*) etc) vary with inter-guide phasing (D) which is scanned at 1 kHz in this example. For reference, the plasma current, line-averaged and edge electron density, the position of the upper hybrid resonance and density gradient scale length for this discharge have already been shown in figure 3. Several observations can be made. First, the coupled power clearly depends upon the phase between the two waveguides. The continuous phase scan allows the amplitude and phase of the reflected waves to be measured as a function of the inter-guide phase shift. Second, the coupling also depends upon the plasma and presumably the conditions in front of the antenna. Thus, the coupling can be measured and studied for conditions which range from vacuum (before and after the discharge) to standard plasmas with large fluctuations in the edge and to the relatively quiet PPCD plasmas. In what follows, we begin by benchmarking the measurements in vacuum against the predictions of the code and then proceed to the plasma case.

4.1. Vacuum reflection

Vacuum reflection is measured with antenna broadcasting into the empty MST vessel. The quantitative agreement with computations is an important validation of both the experimental calibration and the predictive codes. Figure 6(*a*) shows the measured reflection coefficient $(R_1 + R_2)/(F_1 + F_2)$ versus inter-guide phasing for several cases. The value expected from modeling and measured reflection for the antenna positioned flush with the wall with no BN cover are in quantitative agreement for all phases, and the minimum of reflection occurs at $\Phi_{F_1F_2} = 0$. This case matches best the modelled situation. The R/F values for the antenna with a flat BN cover (1.5 mm thick, positioned 4.5 mm from the end of the copper antenna) are also plotted versus the inter-guide phase in figure 6(*a*). Although bench measurements show the BN cover is nearly transparent to 3.6 GHz waves (98% transmission), the reflection coefficient is measurably higher at all phases, with the difference dependent on phase. A second cover, designed to resist deterioration with long term exposure to the plasma [31], is slightly thicker (3.2 mm with 1.6 mm deep grooves milled perpendicular to the wave electric field) and has also been tested. The minimum is still at zero phasing, the reflection coefficient is also higher than for no-cover case and the deviation increases as the phase moves away from the optimum value. The vacuum reflection is mainly determined by the boundary condition at the antenna opening, so the BN cover is expected to have an influence on the vacuum reflection. For oblique launch the effect of the cover on reflection increases with inter-guide phasing, since

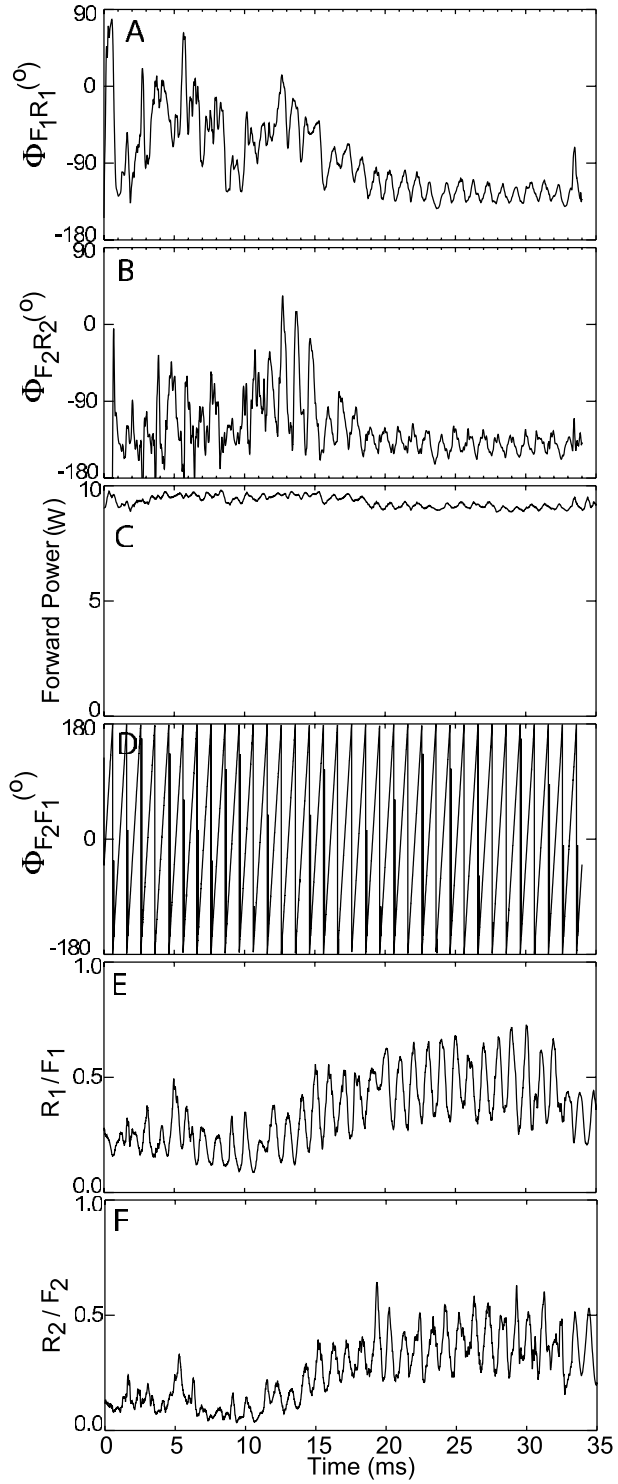

Figure 10. Typical evolution for relevant rf signals on MST, X-mode launch, from the upper to the lower traces: phase between forward and reflected waves in arm 1, phase between forward and reflected waves in arm 2, total forward power, inter-guide phase, reflection in waveguide 1 and reflection in waveguide 2.

the waves encounters a thicker layer of the cover material for larger launch angles.

A second deviation from modelling is caused by changing the location of the antenna with respect to the inner MST wall (δ in figure 4). The effect of the variation of δ was investigated

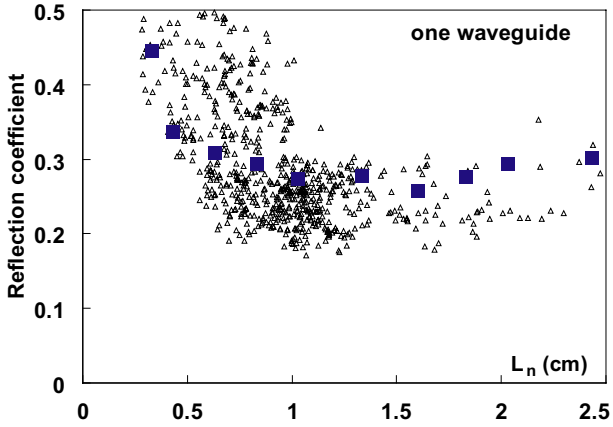

Figure 11. Power reflection coefficient from simulations (blue squares) and experimentally measured (triangles) versus density scale length at UHL for single waveguide, X-mode launch at 10 W.

by measuring the reflection in vacuum versus inter-guide phasing for an uncovered antenna with $\delta = -1$ cm, $\delta = 0$ cm and $\delta = 1$ cm, as illustrated in figure 6(*b*). The minimum of the reflection coefficient versus inter-guide phasing occurs at zero phase for all δ, but the reflection coefficient for non-optimum phases is quite sensitive to the antenna position: up to 5% change (35% relative change) for 1 cm ($\sim \lambda/8$) position change.

4.2. Coupling to the plasma

The same experimental approach was used to study the coupling to the plasma at a frequency of 3.6 GHz. Practical concerns have required that the antenna position be slightly behind the MST wall and that a dielectric cover be installed (figure 4) for most of the experiments discussed below. Dependence of the reflection and phase on the edge density conditions and inter-guide phasing are investigated for different plasma conditions (standard plasma and low fluctuation regime) and different polarizations (X- and O-mode).

Single waveguide reflection was investigated using the twin waveguide antenna in the X-mode with one passive arm and power launched through the other arm. The reflection coefficient is shown in figure 11, with the measured R/F values plotted versus density scale length (L_n) over the typical experimental values of $\sim$ 0.5 to 3.5 cm. The experimental values agree with the expected values (also shown) to within the statistical spread of the data.

A similar study of reflection versus density scale length was performed by launching power in both arms of the twin waveguide antenna. In order to isolate the influence of the density profile on the reflection coefficient, the optimum inter-guide phase was selected. The reflection coefficient at Φ_{opt} is plotted versus the measured density scale-length in figure 12. The theoretical predictions for reflection at varying L_n are also plotted, and the experimental data again agree with the modelling. From these data, it is clear that the optimal coupling can be achieved in target plasmas with a $L_n \sim 0.8$–1.5 cm; these values are typical in the reduced-fluctuation periods. Both theory and measurements show that the phased array

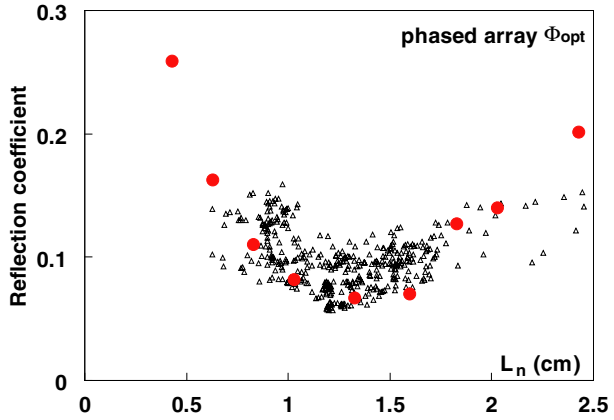

Figure 12. Power reflection coefficient from simulations (red circles) and experimentally measured (triangles) versus density scale length at UHL for twin waveguide at optimum phase, X-mode launch at 10 W.

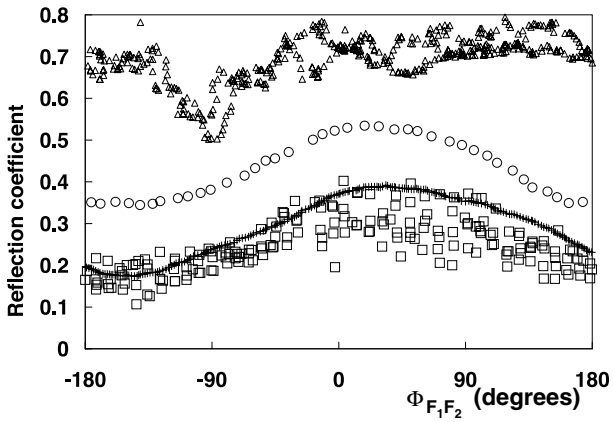

Figure 13. Measured power reflection coefficient versus phase between waveguides for a 3.6 GHz X-mode wave at 1W (□) and 50 kW (×) launched in a 190 kA PPCD regime plasma with BN cover, PPCD plasma with no cover 1 W (△), standard plasma 1 W (○).

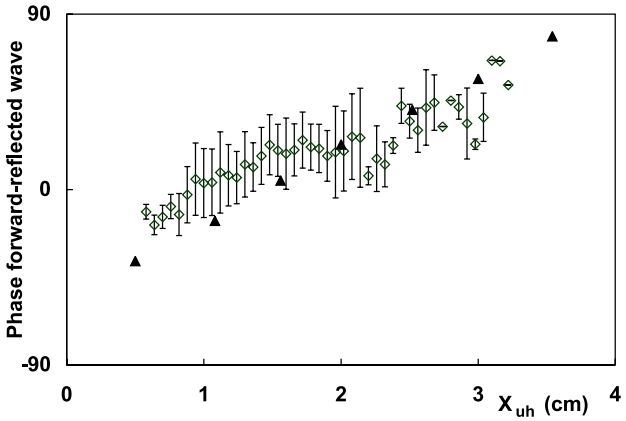

Figure 14. Phase between forward and reflected wave versus the position of the UHL (rhombs) with the standard deviations also represented. Phase predicted by theory is plotted with triangles.

reflection coefficient is considerably lower (by up to ~ 0.2 representing less than 50%) than the single waveguide case plotted in figure 11 and demonstrate the sensitivity of coupling to the edge density profile.

The dependence of the reflection on the inter-guide phasing was investigated in experiment using a continuous phase scan. The edge density conditions during the phase scan were carefully selected so that $L_n \sim 1.4$ cm, $x_{\mathrm{uh}} \sim 3.5$ cm and $I = 190$ kA are almost constant. For O-mode polarization (figure 7), the simulation and experimental data both show a minimum at, and symmetry about, zero phase. The experimental values are slightly lower than the predicted, but this is not surprising as the simulation does not consider the effect of the BN cover.

The X-mode launch into similar plasmas was studied in more detail. For the case when no cover was used in front of the antenna (in figure 13) the X-mode reflection shows a weak minimum near the expected -85°, although the overall reflection is quite high. The reflection coefficient with a covered antenna is much lower (around 10%), nearing that of the simulation, but the minimum is shifted significantly to about -150°. The change in reflection with the cover is probably due to two effects: first, the cover physically blocks plasma from entering the antenna, and it may act as a limiter to modify the density profile (Langmuir probe density measurements are displaced ~ 1 m from the antenna). The symmetry about $\Phi_{F_1F_2} = 0$ is not expected or measured for X-mode launch. The shape of the X-mode reflection versus phase curve is robust—it is observed in higher fluctuation plasma (although the magnitude of the reflection is higher) and the shape is also reproduced at higher launch power, with similar R/F and optimum phase values at 50 kW launched.

The phase between the reflected and the forward-travelling waves (Φ_{FR}) is expected to increase with the distance from the antenna to the UHL. This is illustrated for the case of single-guide launch (other arm passive) as a plot of Φ_{FR} versus x_{uh} in figure 14. The increase in phase with upper hybrid position is about 60° cm^{-1} for the measured values (to within an arbitrary constant), while the theoretical prediction for the same conditions (also plotted in figure 14) show a similar slope. The expected trend is observed and with improved modeling this could be used as a reflectometry-based edge density diagnostic in future work.

The effects of the antenna positioned slightly behind the MST wall and the presence of the dielectric cover are not incorporated in modelling, and deviations from quantitative agreement with experimental results are expected. Primary results of the experiment are in qualitative agreement with the modelling. The coupling to the electromagnetic waves propagating in plasma is sensitive to the edge density profile and inter-guide phasing. The polarization of the launched wave (X-mode or O-mode) affects the optimum launch angle and coupling. The phase shift between the reflected and forward power in each arm does not exactly match the predicted values but does follow the expected trend with the change in the position of the upper hybrid resonance.

5. Conclusions

The EBW plays a role in ECRF plasma heating in the tokamak, stellarator and spherical torus. In this work, the conditions for reducing reflection of ECRF waves in the RFP in order to increase coupling to the EBW have been investigated

theoretically and experimentally. Simulations show that a phased array waveguide antenna is suitable for coupling power from ECRF to the EBW within the overdense RFP plasma. Experiments show that the optimal launching geometry for coupling ECRF to the RFP plasma is a waveguide grill with BN cover, and X-mode launching at a particular inter-guide phase Φ_{opt} .

Several phenomena predicted by simulations have been experimentally verified by analysing the amplitude and phase of reflected waves. The coupling is very sensitive to the edge electron density profile. There is quantitative agreement between the expected and measured reflection amplitude versus density scale length and between the expected and measured phase of the reflected wave versus position of the UHL.

Optimum coupling (lowest reflection) occurs for a particular inter-guide phase (oblique launch angle) from the twin waveguide antenna; the optimum phase depends on several variables. In O-mode launch, the optimum is at 0° (normal launch) and symmetry about zero is both predicted and measured. A lower overall reflection is possible for phased waveguide array X-mode launch, and the optimum phase depends on L_n, frequency of the launched wave and other variables, with a typical predicted optimum near -90°. The experimental power reflection coefficient in X-mode is not symmetric about zero phasing in both experiment and theory. There are discrepancies between the values of the X-mode reflection at positive phasing attributed to the limitations of the theoretical model.

The edge density profile during the low-fluctuation periods of MST low current discharges has an L_n very close to the optimum value for coupling power. For appropriate phasing in X-mode launch into the target density profile, reflection coefficients less than 15% are routinely measured.

Acknowledgment

This work is supported by the US Department of Energy.

References

[1] Bernstein I.B. 1958 *Phys. Rev.* **109** 10
[2] Preinhaelter J. and Kopecký V. 1973 *J. Plasma Phys.* **10** 1
[3] Nakajima S. and Abe H. 1988 *Phys. Rev.* A **38** 4373
[4] Petrillo V., Lampis G., Maroli C. and Riccardi C. 1989 *Phys. Fluids* B **1** 1396
[5] Pinsker R.I., Carter M.D., Forest C.B., Svidzinski V.A. and Chattopadhyay P.K. 2005 *Plasma Phys. Control. Fusion* **47** 335
[6] McWilliams R., Edrich D., Wolf N.S. and Brusati M. 1992 *Nucl. Fusion* **32** 687
[7] Kuehl H.H., O'Brien B.B. and Stewart G.E. 1970 *Phys. Fluids* **13** 1595
[8] O'Brien B.B. and Kuehl H.H. *Phys. Fluids* 1971 **14** 1187
[9] Yadav V.K. and Bora D. 2004 *Phys. Plasmas* **11** 4582
[10] Robinson P.A. 1987 *J. Plasma Phys.* **37** 449
[11] Sugawa M. 1988 *J. Plasma Phys* **40** 87
[12] Maroli C., Petrillo V., Lampis G. and Basilico F. 1992 *Phys. Fluids B-Plasma* **4** 1836
[13] Sugai H. 1981 *Phys. Rev. Lett.* **47** 1899
[14] Armstrong R., Rasmussen J.J., Stenzel R.L. and Trulsen J. 1981 *Phys. Lett.* **85** 281
[15] Forest C., Chattopadhyay P.K., Harvey R.W. and Smirnov A.P. 2000 *Phys. Plasmas* **7** 1352
[16] Taylor G *et al* 2004 *Phys. Plasmas* **11** 4733
[17] Shevchenko V., Baranov Y., O'Brien M. and Saveliev A. 2002 *Phys. Rev. Lett.* **89** 265005
[18] Forest C.B., Harvey R.W. and Smirnov A.P. 2001 *Nucl. Fusion* **41** 619
[19] Laqua H.P., Maassberg H., Marushchenko N.B., Volpe F., Weller A. and Kasparek W. 2003 *Phys. Rev. Lett.* **90** 075003/1
[20] Volpe F. and Laqua H.P. 2003 *Rev. Sci. Instrum.* **74** 1409
[21] Pinsker R.I., Carter M.D. and Forest C.B. 2001 *Radio Frequency Power in Plasmas: 14th Topical Conf. (Oxnard, CA, USA)* (New York: American Institute of Physics) p 350
[22] Forest C.B. *et al* 2003 *Proc. 12th Joint Workshop on Electron Cyclotron Emission and Electron Cyclotron Heating (EC-12) (Aix-en-Provence, France)* (New York: American Institute of Physics) ed G. Giruzzi (Singapore: World Scientific) p 17
[23] Chattopadhyay P.K., Anderson J.K., Biewer T., Craig D., Forest C.B., Harvey R.W. and Smirnov A.P. 2002 *Phys. Plasmas* **9** 752
[24] Brambilla M. 1976 *Nucl. Fusion* **16** 47
[25] Chapman B.E. *et al* 2002 *Phys. Plasmas* **9** 2061
[26] Dexter R., Kerst D., Lovell T., Prager S. and Sprott J. 1991 *Fusion Technol.* **19** 131
[27] Sarff J.S. *et al* 2003 *Nucl. Fusion* **43** 1684
[28] Ram A.K. and Schultz S.D. 2000 *Phys. Plasmas* **7** 4084
[29] Jaeger E.F., Carter M.D., Berry L.A., Batchelor D.B., Forest C.B. and Weitzner H. 1998 *Nucl. Fusion* **38** 1
[30] Choi D.W., Powers E.J., Bengtson R.D., Joyce G., Brower D.L., Luhmann N.C. and Peebles W.A. 1986 *Rev. Sci. Instrum.* **57** 1989
[31] Anderson J.K., Cengher M., Cox W.A., Forest C.B., McMahon S.M., Pinsker R.I. and Svidzinski V. 2005 *Radio Frequency Power in Plasmas: 16th Topical Conf. (Park City, Utah, USA)* ed S.J. Wukitch and P.T. Bonoli (New York: American Institute of Physics) p 341